Acta Oceanol. Sin., 2019, Vol. 38, No. 1, P. 172–179
https://doi.org/10.1007/s13131-019-1382-x
http://www.hyxb.org.cn
E-mail: hyxbe@263.net

Performances of conventional fusion methods evaluated for inland water body observation using GF-1 image

Yong Du[1, 3], Xiaoyu Zhang[1]*, Zhihua Mao[2], Jianyu Chen[2]

[1] School of Earth Sciences, Zhejiang University, Hangzhou 310027, China

[2] State Key Laboratory of Satellite Ocean Environment Dynamics, Second Institute of Oceanography, Ministry of Natural Resources, Hangzhou 310012, China

[3] School of Biology and the Environment, Jiyang College of Zhejiang A&F University, Zhuji 311800, China

Received 29 August 2017; accepted 22 December 2018

Abstract

Satellite remote sensing of inland water body requires a high spatial resolution and a multiband narrow spectral resolution, which makes the fusion between panchromatic (PAN) and multi-spectral (MS) images particularly important. Taking the Daquekou section of the Qiantang River as an observation target, four conventional fusion methods widely accepted in satellite image processing, including pan sharpening (PS), principal component analysis (PCA), Gram-Schmidt (GS), and wavelet fusion (WF), are utilized to fuse MS and PAN images of GF-1. The results of subjective and objective evaluation methods application indicate that GS performs the best, followed by the PCA, the WF and the PS in the order of descending. The existence of a large area of the water body is a dominant factor impacting the fusion performance. Meanwhile, the ability of retaining spatial and spectral informations is an important factor affecting the fusion performance of different fusion methods. The fundamental difference of reflectivity information acquisition between water and land is the reason for the failure of conventional fusion methods for land observation such as the PS to be used in the presence of the large water body. It is suggested that the adoption of the conventional fusion methods in the observing water body as the main target should be taken with caution. The performances of the fusion methods need re-assessment when the large-scale water body is present in the remote sensing image or when the research aims for the water body observation.

Key words: GF-1 satellite image, fusion methods, fusion evaluation, inland water body

Citation: Du Yong, Zhang Xiaoyu, Mao Zhihua, Chen Jianyu. 2019. Performances of conventional fusion methods evaluated for inland water body observation using GF-1 image. Acta Oceanologica Sinica, 38(1): 172–179, doi: 10.1007/s13131-019-1382-x

1 Introduction

As mother river of Zhejiang Province, the Qiantang River is famous for its turbulent astronomical tide with the maximum tide flow rate of approximately 12 m/s (Zeng, 2011). The violent flows of the tidal bore erode riverbed and result in sharply increased suspended sediment concentration, the turbidity maximum zone forms from Ganpu to Cangqian, especially from Caoejiang Estuary to Yanguan, the highest suspended sediment concentration reported is 65.8 kg/m^3 near Daquekou (Pan et al., 2013). The turbulent hydrodynamic environment exerts a series of social and ecological environmental problems including bank erosion, deposition reclamation and water quality decay. The channel security is also an important local issue. However, conventional hydrodynamic and aquatic eco-environmental monitoring is insufficient for such a wide array of issues. As an important supplementary tool of traditional monitoring, satellite remote sensing technology provides not only advantages such as large scale, speedy and low cost observation but also possibility for long-term ambulatory monitoring (Malthus et al., 2012).

Satellite data used for inland or estuarine water monitoring are mainly multi-spectral data with high spatial resolution, such as Landsat TM/ETM+ (Thematic Mapper/Enhanced Thematic Mapper Plus) (Carpintero et al., 2013), SPOT (Systeme Probatoired' Observation dela Tarre) (Casal et al., 2011), IKONOS (Ekercin, 2007), WorldView-2 (Concha and Gerace, 2012; Eugenio et al., 2013) and HJ-1 A/B CCD (Nazeer and Nichol, 2015). Multi-spectral (MS) data fused with panchromatic (PAN) data are widely used in digital image analysis and comparison that allow users to obtain more clear images. There are various types of fusion methods, such as intensity-hue-saturation transform (IHS) (Carper et al., 1990), brovey transform (BT) (Mandhare et al., 2013), GS (Karathanassi et al., 2007), PCA (Jia, 1998; Metwalli et al., 2009), PS (Zhang, 2002a) and WF (Li et al., 1999). Up to date, such fusion algorithms are developed and evaluated basically for classification improvement of terrestrial remote sensing, enhancement of land change detection and more. For different physical imaging mechanisms between terrestrial and aquatic remote sensing (e.g., water body is usually darker than land objects for the strong absorption of visible wavelengths, and the reflectivity of one pixel usually embodies comprehensive kinds of water

Foundation item: The National Key Research and Development Program of China under contract Nos 2016YFC1400901 and 2018YFC1406600; the National Natural Science Foundation of China under contract No. 40706057; the Environmental Protection and Science and Technology Plan Project of Zhejiang Province of China under contract No. 2013A021; the Research Center for Air Pollution and Health of Zhejiang University.

*Corresponding author, E-mail: Zhang_xiaoyu@zju.edu.cn

color parameters), irrational transplant with the fusion algorithms which are generally adopted for land will hamper the accurate quantitative inversion of aquatic eco-environmental parameters. Furthermore, the particular spectral characteristics of the water body require a high signal-to-noise ratio and multiband design with narrowband width of satellite data, and high spatial resolution is necessary for satellite data when aiming for the inland water body observation. Therefore, fusion between MS data and high spatial resolution PAN data is especially significant in this case.

The Daquekou section is the bottleneck of the waterway from the Qiantang River to the Hangzhou Bay. To effectively monitor the complex hydrodynamic environment, GF–1 satellite images with the high spatial resolution are utilized in this study. As the first high resolution satellite of China's earth observation system, GF–1 realizes effectively the combination of multispectral with high spatial and temporal resolution of optical remote sensing technology. The ability of retrieving inland water information of GF–1 has been demonstrated (Zhu et al., 2015).

This study has done the following work: (1) four conventional fusion methods, including PS, PCA, GS and WF, are employed for the fusion of 2 m PAN and 8 m MS GF–1 data; (2) subjective and objective evaluation methods are established to evaluate the performance of the fused images, and suitable fusion methods for GF–1 in this study are then decided; and (3) the possible influencing factors of the fusion effect are analyzed. The study will be beneficial to the observation of the suspended sediment concentration and their transportation routine in the Daquekou section which will give powerful evidence for the hydrodynamic condition in this concerned area. The study will also help with the rapid determination of appropriate fusion methods for similar researches.

2 Data and methods

2.1 *GF–1 image*

GF–1 satellite was launched on April 26, 2013. It operates at an altitude of 645 km in a sun-synchronous orbit. Detailed technical parameters are listed in Table 1. The spatial resolution of GF–1 is lower than that of WorldView–2, but their spectral ranges and widths are basically the same. With a wider spatial coverage than WorldView–2, the advantages of GF–1 are obvious in observing turbulent hydrodynamic environment of the inland water body.

The GF–1 image utilized in this study is L1A0000112890 (November 18, 2013), covering an area centered at 30.2°N, 120.7°E around Daquekou Bay of the Qiantang River (Fig. 1). The water area is about 45% of the whole image, with the narrowest width of about 2.3 km near Yanguan and the widest width of about 12 km near Ganpu. The average water depth in this area is about ~4 m (Pan et al., 2013). There are shoals at Nianerduan in the south shore and from Daquekou to Dajianshan in the north shore. The shoals narrow the river, causing the flow rate to increase rapidly. High concentration of suspended sediment carried by the river and re-suspension from bottom will perform rich image textural characteristics.

Table 1. Technical parameters of GF–1 and WorldView–2

Image	Spatial resolution/m	Spectral range/μm	Width/km	Revisit time/d
GF–1	PAN 2	PAN 0.45–0.90	PAN 60	41
	MS 8/16	8 m /16 m MS	MS 60/800	4
		0.45–0.52		
		0.52–0.59		
		0.63–0.69		
		0.77–0.89		
World-View–2	PAN 0.46	PAN 0.45–1.04	16.4	1.1
	MS 1.84	MS 0.49–0.51 (blue)		
		0.51–0.58 (green)		
		0.63–0.69 (red)		
		0.77–0.89 (near-infrared)		

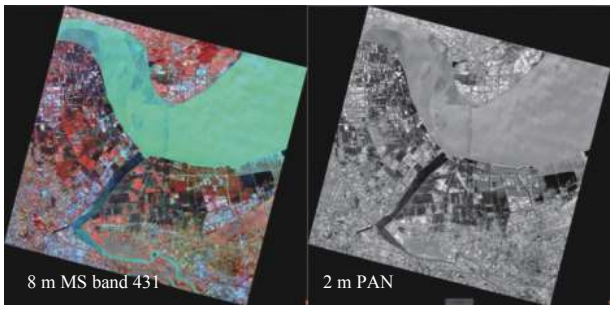

Fig. 1. Images of the study area.

2.2 *Optimal bands triplet*

In this study, we adopt an optimum index factor (OIF) to extract the maximum amount of information from different spectra (Chavez et al., 1982) of GF-1 multi-spectral data. The concept behind the OIF is that smaller pair-wise correlation produces a larger standard deviation within a band, and thus provides more information. The OIF I_0 is computed as follows:

$$I_0 = \sum_{i=1}^{3} S_i / \sum_{j=1}^{3} R_{ij}, \quad (1)$$

where S_i is the standard deviation of band i, and R_{ij} is the pair-wise correlation coefficient for bands i and j. A high OIF value indicates more information captured.

Table 2 shows that all top three optimal band triplets contain the 4th (NIR) band. The reason is that the 4th band has a larger standard deviation, and its correlations with other bands are small. According to the OIF scores, the combination of 1st, 3rd and 4th bands that have the highest OIF of 97.003 is selected as the optimum band combination in this study.

Table 2. Calculation results of the optimum index factor

Ranking	Band combination	OIF
1	Band 431	97.003
2	Band 432	96.566
3	Band 421	81.610
4	Band 321	38.725

2.3 *Fusion methods*

The PS, PCA, GS and WF methods are conventional pixel-level fusion methods, performing excellently especially in high-resolution remote sensing images. The principles are listed as follows.

2.3.1 *The PAN sharpening (PS)*

The PS combines a high spatial resolution PAN image with a

low spatial resolution MS image to enhance the spatial resolution using a least squares method. This method retains the spectral characteristics by preserving the mean, standard deviation and histogram shape for each band (Zhang, 2002a, b), and it automatically aligns PAN data and MS data to successfully retain spectral information, increases the spatial resolution and highlights ground information.

From Guo (2015), PS is expressed as

$$DN_{\mathrm{MS}}^{\mathrm{h}}(\Omega_n)=\frac{DN_{\mathrm{PAN}}^{\mathrm{h}}(\Omega_n)}{DN_{\mathrm{PAN}}^{\mathrm{l}}(\Omega_n)}DN_{\mathrm{MS}}^{\mathrm{l}}(\Omega_n), \tag{2}$$

where $DN_{\mathrm{PAN}}^{\mathrm{h}}(\Omega_n)$ is the digital number of the pixel of a high spatial-resolution image, $DN_{\mathrm{PAN}}^{\mathrm{l}}(\Omega_n)$ can be obtained from $DN_{\mathrm{PAN}}^{\mathrm{h}}(\Omega_n)$ by resampling, $DN_{\mathrm{MS}}^{\mathrm{l}}(\Omega_n)$ represents the digital number of the pixel of a low spatial resolution image, and $DN_{\mathrm{MS}}^{\mathrm{h}}(\Omega_n)$ is the digital number of the pixel of the multi-spectral image with a high spatial resolution.

2.3.2 *The principal component analysis (PCA)*

PCA, also called Karhunen-Loeve transform (K-L transform) (Kang et al., 2008), transforms a number of correlated variables from MS bands into a small number of uncorrelated linear combinations of variables called principal components (Chavez and Kwarteng, 1989; Pohl and van Genderen, 1998). The PCA is based on the statistical characteristics of a multiband orthogonal linear transform (Chavez et al., 1991). The PCA has no band limitations, and achieves an improved retention of spectra (Cetin and Musaoglu, 2009; Kang et al., 2008). Moreover, the first principal component contains maximum information from the original image and can substantially change the hue.

A transform matrix is needed for the image fusion as follows:

$$Y=TX, \tag{3}$$

where X is the pixel matrix of the original multi-spectral image band, T is the principal component transform matrix and Y is the pixel matrix of every principal component after the K-L transformation.

The covariance matrix $\left(\sum Y\right)$ of the principal component pixel (Y) is as follows:

$$\sum Y=\begin{pmatrix} \lambda_1 & 0_{12} & \cdots & 0_{1n} \\ 0_{21} & \lambda_2 & & \vdots \\ \vdots & & & 0_{m-1,\,n} \\ 0_{m1} & \cdots & 0_{m,\,n-1} & \lambda_n \end{pmatrix}, \tag{4}$$

where $\lambda_1, \lambda_2 \ldots, \lambda_n$ are the covariance matrix eigenvector of the original multi-spectral image (Sun, 2002; Wang and Jiang, 2015).

2.3.3 *The Gram-Schmidt process (GS)*

The GS was developed by Laben and Brower (Laben and Brower, 2000), which is similar to the PCA in terms of application technology (Hauter et al., 1997; Karathanassi et al., 2007). The difference between the GS and the PCA is that the information is mainly concentrated in the first principal component after the PCA, but an orthogonal transform is applied in the GS process and then the information of each component does not change after the transformation. The GS process was designed for high spatial resolution images and is suitable for images with any number of bands because of its capability in retaining spatial texture information (Aiazzi et al., 2006; Huang, 2011; Karathanassi et al., 2007).

The basic process of the GS is as follows (Ha et al., 2013):

$$\begin{cases} P_{\mathrm{GS},\,T}(i,j)=[B_T(i,j)-\mu_T]-\sum_{l=1}^{T-1}[\phi(B_T,\,P_{\mathrm{GS},\,l})\cdot P_{\mathrm{GS},\,l}(i,j)], \\ B_T(i,j)=[P_{\mathrm{GS},\,T}(i,j)+\mu_T]+\sum_{l=1}^{T-1}[\phi(B_T,\,P_{\mathrm{GS},\,l})\cdot P_{\mathrm{GS},\,l}(i,j)], \\ \mu_T=\dfrac{\sum_{j=1}^{N}\sum_{i=1}^{M}B_T(i,j)}{M\cdot N}, \\ \phi(B_T,\,P_{\mathrm{GS},\,l})=\left[\dfrac{\sigma(B_T,\,P_{\mathrm{GS},\,l})}{\sigma(P_{\mathrm{GS},\,l},\,P_{\mathrm{GS},\,l})^2}\right], \end{cases} \tag{5}$$

where $P_{\mathrm{GS},\,T}$ is the T orthogonal component after GS transform; B_T is the T band of the original satellite image with a low spatial resolution; μ_T is the mean grey degree of the pixel of T band of an original low spatial resolution image; $\phi(B_T,\,P_{\mathrm{GS},\,l})$ is the covariance of the K band of the original low spatial resolution image and $P_{\mathrm{GS},\,l}$; i and j are the index of rows and columns of the original low spatial resolution image, respectively; and M and N are the numbers of rows and columns of the whole image, respectively.

2.3.4 *The wavelet fusion (WF)*

The WF is based on the principle of wavelet decomposition of an image and can extract spatial details from a PAN image to incorporate an MS image, which can minimize colour distortion. The wavelet decomposition of MS remote sensing image and high spatial resolution PAN image can be done based on Eq. (6), to obtain the approximation components and the details of the image. Then, the fusion could be carried out respectively. Finally, the fused image can be obtained with an inverse wavelet transform of the approximation components and the details of the image.

$$\begin{cases} Y_{m,\,n}^{a}=\dfrac{1}{2}\sum_{k,\,I\in Z}Y_{k,\,I}^{a+1}h_{k-2m}h_{k-2n}, \\ d_{m,\,n}^{a1}=\dfrac{1}{2}\sum_{k,\,I\in Z}Y_{k,\,I}^{a+1}h_{k-2m}g_{k-2n}, \\ d_{m,\,n}^{a2}=\dfrac{1}{2}\sum_{k,\,I\in Z}Y_{k,\,I}^{a+1}g_{k-2m}h_{k-2n}, \\ d_{m,\,n}^{a3}=\dfrac{1}{2}\sum_{k,\,I\in Z}Y_{k,\,I}^{a+1}g_{k-2m}g_{k-2n}, \end{cases} \tag{6}$$

where m and n are the location indexes of the pixel; Y^a (the subscripts are the spatial scale) is the low frequency approximation component of the image Y^{a+1}; $d_{m,\,n}^{a1}$, $d_{m,\,n}^{a2}$, $d_{m,\,n}^{a3}$ are the details of the component on vertical, horizontal and diagonal direction of the image Y^{a+1}, respectively (Wang et al., 2015).

The WF can select wavelet base and layer number of the wavelet transform according to different characteristics of the input image, and can import image details based on specific requirements. The WF considers spatial detail of the processed image, but it also produces certain spectral degradation (King and Wang, 2001; Ranchin and Wald, 1993).

3 Fusion performance assessment

Before fusion, both PAN and MS images are processed with a

geometric registration. The registration error is controlled in 0.5 pixel to ensure fusion performance.

The GF-1 images fused by the PS, GS, PCA and WF are shown in Fig. 2. They are assessed using subjective and objective assessment methods.

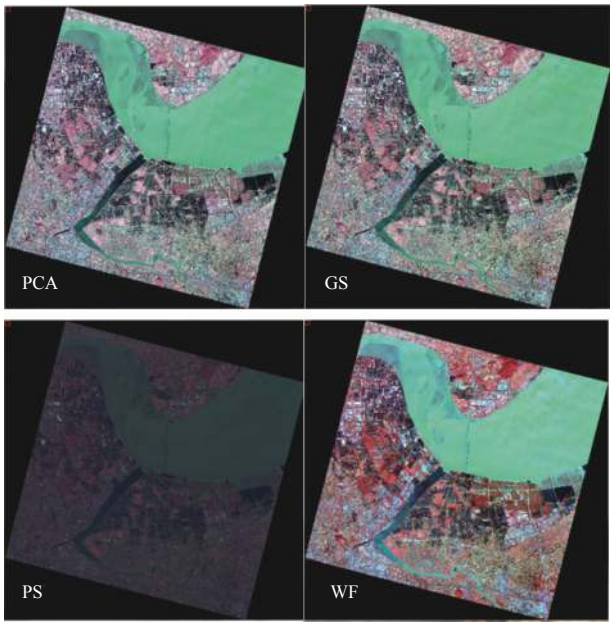

Fig. 2. Four fusion performance of GF-1 image.

3.1 *Subjective assessment*

A subjective assessment relies on the perception of human eyes in colour, clarity, spectral information, and texture information. The rules of the subjective assessment are as follows: the fused image should be clear, not fuzzy; the whole brightness and colour of the fused image should make observers feel comfortable; and the fused image should present the important features and the spatial information of the original image.

We can see at the first sight of Fig. 2 that the PS is not suitable for this study, although it is widely used (e.g., Guo et al., 2015; Liu et al., 2015). There is an obvious decline in brightness after the PS inducing the loss of suspended sediment information.

The texture of the water body is more abundant after processing with the GS, the WF and the PCA. To get better visual judgment, the fusion images obtained by the GS, the WF and the PCA are magnified and tailored Fig. 3). Figure 3 demonstrates that the image processed with the WF is blur. Furthermore, the brightness and clarity of the road in the GS fusion image are better than those in the PCA fusion image.

3.2 *Objective assessment*

3.2.1 *Objective assessment indexes*

In this study, we primarily employ the statistical indexes (Huang et al., 2012; Liu, 2010; Liu and Zhao, 2008; Wei and Li, 2003) shown in Table 3 to perform an objective evaluation. The mean and correlation coefficient indexes are used to indicate spectral information inheritance ability. Standard deviation, average gradient, entropy, and cross entropy demonstrate the in-

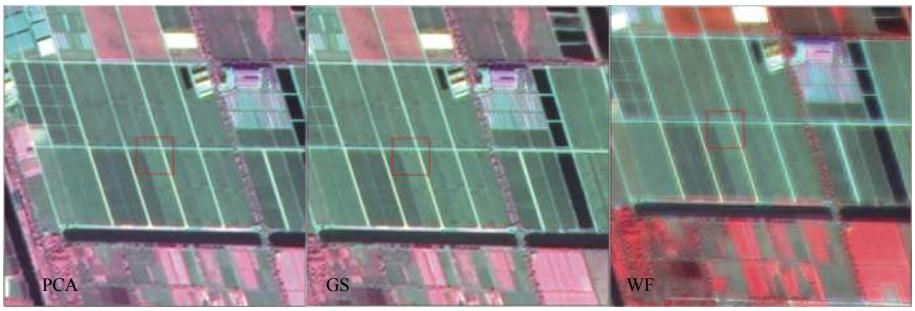

Fig. 3. Fusion results of GF-1 image by three types of fusion methods.

Table 3. Introduction of the objective evaluation indexes

Classification	Index	Formula	Scoring rules
Evaluation indexes based on the statistical characteristics of a single image	mean	$\hat{\mu}(\boldsymbol{F}) = \frac{1}{MN_i}\sum_{i=1}^{M}\sum_{j=1}^{N}F(i,\ j)$	(1) order the six indicators according to the Matlab calculation results; (2) assign each indicator; (3) calculate the total score, the method with the minimum score is the optimal fusion method
	standard deviation (d_{st})	$d_{\mathrm{st}}(\boldsymbol{F}) = \sqrt{\sum_{i=1}^{M}\sum_{j=1}^{N}[F(i,\ j) - \hat{\mu}]^2 / MN}$	
	entropy	$H(\boldsymbol{p}) = -\sum_{i=1}^{n} p_i \log_2 p_i$	
	average gradient	$\overline{G}(\boldsymbol{x},\ \boldsymbol{y}) = \frac{1}{MN}\sum_{i=1}^{M}\sum_{j=1}^{N}\sqrt{\left[\left(\frac{\partial f(x_i,\ y_i)}{\partial x_i}\right)^2 + \left(\frac{\partial f(x_i,\ y_i)}{\partial y_i}\right)^2\right]/2}$	
Evaluation indexes based on the relationship between the source image and the fused image	cross entropy	$D(\boldsymbol{p},\ \boldsymbol{q}) = \sum_{i=1}^{n} p_i \log_2 \frac{p_i}{q_i}$	
	correlation coefficient	$C(\boldsymbol{f},\ \boldsymbol{g}) = \frac{\sum_{i,j}[(f_{i,j} - e_f) \times (g_{i,j} - e_g)]}{\sqrt{\sum_{i,j}[(f_{i,j} - e_f)^2] \times \sum_{i,j}[(g_{i,j} - e_g)^2]}}$	

tegration degree of spatial detail (Guo et al., 2015).

3.2.2 *Objective assessment*

The quality of images after having used the four fusion methods are objectively assessed. To evaluate the influence of existence of the water body on fusion performance, the image with water only and the image with water deducted are also evaluated, respectively. The quantitative results are shown in Table 4. To facilitate the analysis, the statistical data are plot in scatter in Figs 4 and 5. The horizontal dotted lines denote the mean values of the indexes of the original GF–1 PAN and MS images. The similarity between the values of the fusion images and the original GF–1 images is used to evaluate image fusion quality.

3.2.2.1 Assessment of spectral information inheritance

The similarity of the mean values between the fused image and the original image, and the strength of the correlation coefficient both suggest the spectral information inheritance ability of the fusion methods. As shown in Fig. 4, the mean value of the GS fused water image is the closest to the original water image, and the GS fused water image has the highest correlation coefficient, suggesting that GS has the strongest capability in keeping water spectral information. The performance of the PCA is secondary to that of the GS in terms of the water image. The mean value of the WF fused water image is not as close to the original water image as that of the GS; furthermore, the correlation coefficient of the whole image after the WF is the lowest. The performance of the PS is the worst, except for the correlation coefficient value of the whole image.

3.2.2.2 Assessment of integration degree of spatial detail

The Larger standard deviation, the average gradient and the entropy indicate more abundant image spatial information. The cross entropy is the difference of a grey level distribution between a source image and a fused image. A smaller difference suggests more information can be extracted from the source image.

As shown in Fig. 5, considering the four indexes, the PS fusion method is not appropriate for keeping spatial details. The WF performs well in terms of the indexes of entropy and cross entropy, but the standard deviation and average gradient values of the whole image and water deducted image after fusion are greatly reduced, which brings about spatial detail ghosting. Both the GS and the PCA perform well, and the performance of image fusion with the GS is better. Both the GS and the PCA are orthogonal methods. However, the information after the PCA is mainly concentrated in the first principal component, which limits the

Table 4. Results of objective evaluation of GF-1 image

		$\hat{\mu}$	d_{st}	$\overline{G}$	H	D	C	Scores
2 m PAN	A	93.063 6	78.911 3	4.741 6	5.487 7	–	–	–
	B	82.497 9	94.526 9	2.546 1	3.028 8	–	–	–
	C	62.736 4	78.821 3	4.476 3	4.363 6	–	–	–
8 m MS	A	86.663 7	78.617 5	6.517 9	6.072 6	–	–	–
	B	70.815 2	84.134 6	3.038 6	4.440 5	–	–	–
	C	50.937 5	67.005 3	6.253 1	4.700 0	–	–	–
PCA	A	91.550 9	76.978 6	4.561 6	6.003 1	0.410 8	0.923 0	15
	B	71.465 6	85.474 4	2.905 0	4.491 7	0.655 5	0.961 2	14
	C	65.475 5	80.601 1	4.110 8	4.747 5	0.193 2	0.964 5	9
GS	A	94.994 0	79.100 1	4.373 5	6.003 9	0.410 2	0.926 0	10
	B	70.926 3	84.583 1	2.784 2	4.492 6	0.651 6	0.965 6	13
	C	62.386 0	77.609 7	4.280 1	4.733 9	0.190 5	0.964 0	11
PS	A	27.542 4	19.709 0	0.732 1	4.309 9	6.565 5	0.932 7	21
	B	82.986 1	87.851 0	0.380 3	3.278 4	3.397 9	0.944 6	18
	C	19.362 0	20.717 8	0.694 1	3.582 7	3.901 6	0.943 4	24
WF	A	84.484 6	77.031 7	4.128 8	6.077 2	0.369 5	0.914 1	14
	B	68.179 1	81.062 7	3.413 5	4.457 4	0.643 7	0.964 7	15
	C	52.393 2	67.970 6	3.777 7	4.718 4	0.185 2	0.955 2	16

Note: A, B and C stand for the whole image, the water image and the deducted image, respectively; –means no data.

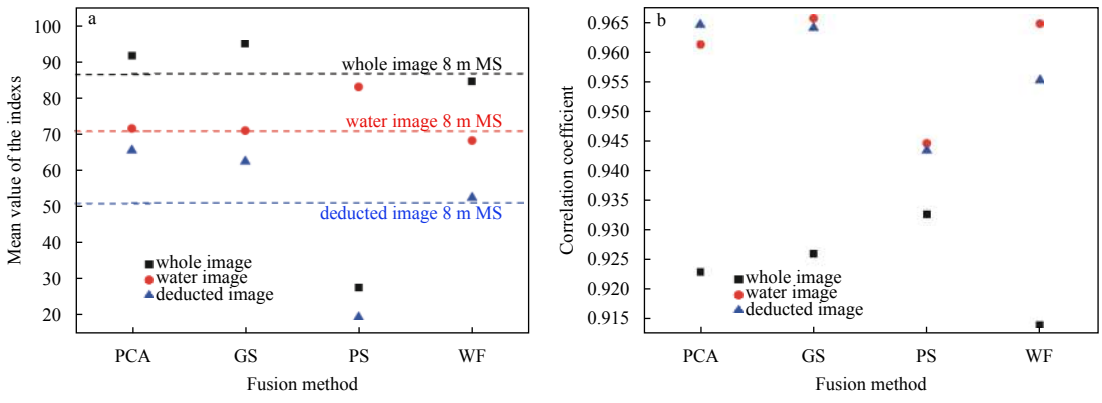

Fig. 4. Distribution of spectral information inheritance index.

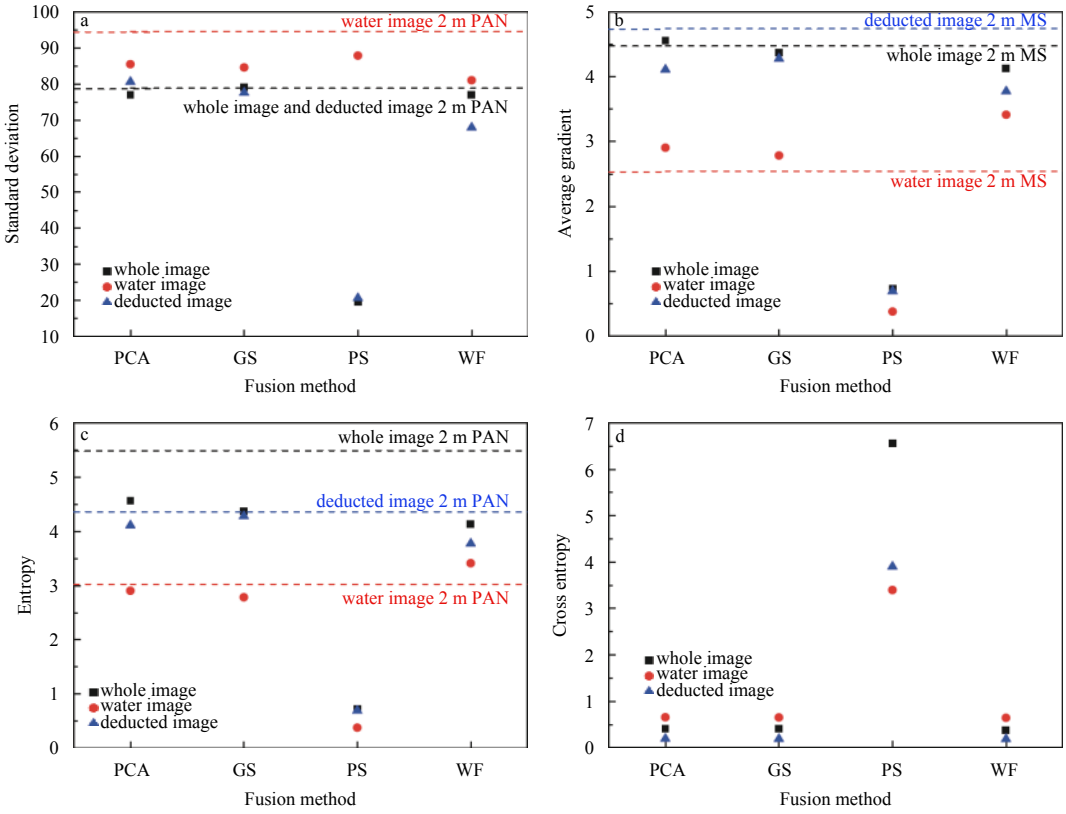

Fig. 5. Distribution of the integration degree of spatial detail index.

ability of the PCA in keeping water spectral information. Each component after the GS is orthogonal, and there is no obvious information difference in each component. Therefore, the fusion image after the GS has the strongest ability in keeping spectral information and improving spatial information (Li et al., 2004; Nikolakopoulos, 2009). Consequently, according to the subjective and objective evaluation results, the GS process is determined as the optimal fusion method.

3.3 *Impact of fusion performance by existence of water body*

Up to date, few studies ever explored the possible influences of different distribution characteristics of terrestrial objects on the performance of a fusion method (Du et al., 2015; Guo, 2015). In this paper, considering the best performance of the GS and the invalidity of the PS, we discuss the possible impacts on the fusion performance induced by the existence of the water body from two aspects:

(1) The fundamental differences of reflectivity acquisition between water and land are the main reason inducing the invalidity of the PS in such cases. When the spatial resolution is high enough, the spectral reflectance curve represents the reflection characteristics of a single terrestrial target. In aquatic remote sensing, the spectral reflectance represents the mixing optical characteristics of water color material no matter how high spatial resolution the image has (Guo, 2015). Equation (2) used by the PS cannot be established for images with a large water area as follows:

$$\frac{DN^{\mathrm{h}}_{\mathrm{PAN}}(\Omega_n)}{DN^{\mathrm{l}}_{\mathrm{PAN}}(\Omega_n)} \neq \frac{DN^{\mathrm{h}}_{\mathrm{MS}}(\Omega_n)}{DN^{\mathrm{l}}_{\mathrm{MS}}(\Omega_n)}. \tag{7}$$

(2) The water body is usually darker than terrestrial objects with the monotonous hue; the former requires a strong capability of keeping spectral information. The GS process has the best spectral information inheritance in the water body image than the other three fusion methods. This may be the reason behind the good performance of GS in this case.

4 Conclusions

To obtain fine observations on aquatic environment in the Daquekou section of the Qiantang River, GF-1 satellite data are pretreated in this study. First, the combination of 1st, 3rd and 4th bands is selected as the optimal band combination by the OIF rule. Then, the 2-m PAN image is fused with 8-m MS image using four fusion methods including the PS, the PCA, the GS and the WF. On the basis of the established subjective and objective assessment methods, at least three preliminary conclusions can be drawn:

(1) The performance of the four fusion methods are listed in the following sequence the GS, PCA, WF and PS. The GS is recommended as the optimum fusion method based on this study. The specificity of spectral characteristics of the water body requires stronger ability of spectral information inheritance. The GS satisfies the requirement most.

(2) Although the PS is widely used in remote sensing image fusion, it is not suitable for GF-1 image fusion aimed at water body observation. The fundamental differences of reflectivity information acquisition between water and land cause the invalidity of the PS, $\frac{DN^{\mathrm{h}}_{\mathrm{PAN}}(\Omega_n)}{DN^{\mathrm{l}}_{\mathrm{PAN}}(\Omega_n)} \neq \frac{DN^{\mathrm{h}}_{\mathrm{MS}}(\Omega_n)}{DN^{\mathrm{l}}_{\mathrm{MS}}(\Omega_n)}$.

(3) The existence of a wide scope of water may be an important factor affecting the performance of the fusion methods. The adoption of conventional fusion methods in the observing water body as the main target should be taken a caution. The perform-

ance of a fusion method needs re-assessment when the large-scale water body is present in the remote sensing image. The work is a preliminary study, which will largely benefit the rapid determination of an efficient fusion method aimed at the inland water body observation.

The processed images are ready for the follow-up sequential inversion of aquatic eco-environmental parameters, including suspended sediment concentration, Chl *a*, etc.

Acknowledgements

We want to express gratitude to the Research Center of High Resolution Satellite Data and Service, at Zhejiang University for GF-1 image data support.

References

Aiazzi B, Baronti S, Selva M, et al. 2006. Enhanced Gram-Schmidt spectral sharpening based on multivariate regression of MS and PAN data. In: 2006 IEEE International Symposium on Geoscience & Remote Sensing. Denver, CO, USA: IEEE, 3806–3809

Carper W J, Lillesand T M, Kiefer R W. 1990. The use of intensity-hue-saturation transformations for merging SPOT panchromatic and multispectral image data. Photogrammetric Engineering & Remote Sensing, 56(4): 459–467

Carpintero M, Contreras E, Millares A, et al. 2013. Estimation of turbidity along the Guadalquivir estuary using Landsat TM and ETM+ images. In: Proceedings Volume 8887, Remote Sensing for Agriculture, Ecosystems, and Hydrology XV. Dresden, Germany: SPIE

Casal G, Sánchez-Carnero N, Sánchez-Rodríguez E, et al. 2011. Remote sensing with SPOT-4 for mapping kelp forests in turbid waters on the south European Atlantic shelf. Estuarine, Coastal & Shelf Science, 91(3): 371–378

Cetin M, Musaoglu N. 2009. Merging hyperspectral and panchromatic image data: qualitative and quantitative analysis. International Journal of Remote Sensing, 30(7): 1779–1804, doi: 10.1080/01431160802639525

Chavez P S Jr, Berlin G L, Sowers L B. 1982. Statistical method for selecting Landsat MSS ratios. Journal of Applied Photographic Engineering, 8(1): 23–30

Chavez P S Jr, Kwarteng A Y. 1989. Extracting spectral contrast in landsat thematic mapper image data using selective principal component analysis. Photogrammetric Engineering & Remote Sensing, 55(3): 339–348

Chavez P S Jr, Sides S C, Anderson J A. 1991. Comparison of three different methods to merge multiresolution and multispectral data: Landsat TM and SPOT panchromatic. Photogrammetric Engineering and Remote Sensing, 57(3): 295–303

Concha J A, Gerace A D. 2012. Atmospheric compensation for WorldView-2 satellite and in-water component retrieval. In: 2012 IEEE International Geoscience and Remote Sensing Symposium. Munich: IEEE, 2833–2826

Du Yong, Zhang Xiaoyu, Huang Dasong, et al. 2015. Evaluation of fusion methods for Worldview-2 aiming to water body observation. Journal of Zhejiang University (Engineering Science) (in Chinese), 49(5): 993–1000

Ekercin S. 2007. Water quality retrievals from high resolution IKONOS multispectral imagery: a case study in Istanbul, Turkey. Water, Air, & Soil Pollution, 183(1–4): 239–251

Eugenio F, Martin J, Marcello J, et al. 2013. Worldview-2 high resolution remote sensing image processing for the monitoring of coastal areas. In: Proceedings of the 21st European Signal Processing Conference (EUSIPCO 2013). Marrakech: IEEE, 1–5

Guo Yulong. 2015. Research of multisource image fusion algorithm for inland water color remote sensing [dissertation] (in Chinese). Nanjing: Nanjing Normal University

Guo Huimin, Hong Yunfu, Li Ying, et al. 2015. Comparison of Fusion methods used for GF–1 satellite image. Geography and Geo-Information Science (in Chinese), 31(1): 23–26

Ha W, Gowda P H, Howell T A. 2013. A review of potential image fusion methods for remote sensing-based irrigation management: Part II. Irrigation Science, 31(4): 851–869, doi: 10.1007/s00271-012-0340-6

Hauter A, Chang K C, Karp S. 1997. Polarimetric fusion for synthetic aperture radar target classification. Pattern Recognition, 30(5): 769–775, doi: 10.1016/S0031-3203(96)00099-4

Huang Dengshan. 2011. Research of pixel-level remote sensing image fusion method[dissertation] (in Chinese). Changsha: Central South University

Huang Hai, Liu Xiangang, Lei Zhigang. 2012. WorldView-2 data fusion methods and evaluation research. Computer Programming Skills and Maintenance (in Chinese), (10): 72–73

Jia Yonghong. 1998. Fusion of Landsat TM and SAR images based on principal component analysis. Remote Sensing Technology & Application (in Chinese), 13(1): 46–49

Kang Tingjun, Zhang Xinchang, Wang Haiying. 2008. Assessment of the fused image of multispectral and panchromatic images of SPOT5 in the investigation of geological hazards. Science in China (in Chinese), 51(S2): 144–153

Karathanassi V, Kolokousis P, Ioannidou S. 2007. A comparison study on fusion methods using evaluation indicators. International Journal of Remote Sensing, 28(10): 2309–2341, doi: 10.1080/01431160600606890

King R L, Wang Jianwen. 2001. A wavelet based algorithm for pan sharpening Landsat 7 imagery. In: Proceedings of the IEEE 2001 International Geoscience and Remote Sensing Symposium. Sydney, NSW, Australia: IEEE, 2: 849–851

Laben C A, Brower B V. 2000. Process for enhancing the spatial resolution of multispectral imagery using pan-sharpening: US, US6011875

Li Cunjun, Liu Liangyun, Wang Jihua, et al. 2004. Comparison of two methods of fusing remote sensing images with fidelity of spectral information. Journal of Image and Graphics (in Chinese), 9(11): 1376–1385

Li Jun, Zhou Yueqin, Li Deren. 1999. Fusion of high-resolution panchromatic and multispectral images by using wavelet transform. Journal of Remote Sensing (in Chinese), 3(2): 116–121

Liu Jianhua. 2010. A comparative study of six methods for the fusion of QuickBird multispectral and pan images in consideration of segmentation effect. Remote Sensing for Land and Resources (in Chinese), 25(3): 21–25

Liu Kun, Fu Jingying, Li Fei. 2015. Evaluation study of four fusion methods of GF-1 pan and mutil-spectral images. Remote Sensing Technology and Application (in Chinese), 30(5): 980–986

Liu Ke, Zhao Wenji. 2008. Evaluation on fusion algorithms of remote sensing image-a case study of SPOT-5. Journal of Capital Normal University (Natural Science Edition) (in Chinese), 29(6): 83–88, 104

Malthus T J, Hestir E L, Dekker A G, et al. 2012. The case for a global inland water quality product. In: Proceedings of the 2012 IEEE International Geoscience and Remote Sensing Symposium (IGARSS). Munich: IEEE, 5234: 5234–5237

Mandhare R A, Upadhyay P, Gupta S. 2013. Pixel-level image fusion using brovey transforme and wavelet transform. International Journal of Advanced Research in Electrical, Electronics & Instrumentation Engineering, 2(6): 2690–2695

Metwalli M R, Nasr A H, Allah O S F, et al. 2009. Image fusion based on principal component analysis and high-pass filter. In: Proceedings of the 2009 International Conference on Computer Engineering & Systems. Cairo: IEEE, 63: 63–70

Nazeer M, Nichol J E. 2015. Combining Landsat TM/ETM+ and HJ-1 A/B CCD sensors for monitoring coastal water quality in Hong Kong. IEEE Geoscience & Remote Sensing Letters, 12(9): 1898–1902

Nikolakopoulos K G. 2009. Spatial resolution enhancement of hyperion hyperspectral data. In: Proceedings of the 2009 1st Workshop on Hyperspectral Image & Signal Processing: Evolution in Remote Sensing. Grenoble: IEEE, 1–4

Pan Cunhong, Zeng Jian, Tang Ziwen, et al. 2013. A study of sediment characteristics and riverbed erosion/deposition in Qi-

antang Estuary. Hydro-Science and Engineering (in Chinese), (1): 1–7

Pohl C, van Genderen J L. 1998. Review article multisensor image fusion in remote sensing: concepts, methods and applications. International Journal of Remote Sensing, 19(5): 823–854, doi: 10.1080/014311698215748

Ranchin T, Wald L. 1993. The wavelet transform for the analysis of remotely sensed images. International Journal of Remote Sensing, 14(3): 615–619, doi: 10.1080/01431169308904362

Sun Danfeng. 2002. Study on fusion algorithms of IKONOS pan and multi-spectral images. Remote Sensing Technology and Application (in Chinese), 17(1): 41–45

Wang Xiaomian, Jiang Yun. 2015. GF-1 Satellite for remote sensing image fusion and quality assessment methods. Geomatics & Spatial Information Technology (in Chinese), (8): 178–179

Wang Ting, Liao Xiuying, Cheng Hui. 2015. Evaluation on data quality of GF-1 PMS sensor data in Youxian, Hunan Province. Progress in Geophysics (in Chinese), 30(5): 2082–2088

Wei Jun, Li Bicheng. 2003. Remote-sensing image fusion based on IHS transform, wavelet transform and high pass filtering. Journal of Information Engineering University (in Chinese), (2): 46–50

Zeng Jian. 2011. Data mining-based characteristics of flow and sediment transport in Qiantang Estuary [dissertation] (in Chinese). Hangzhou: Zhejiang University

Zhang Yun. 2002a. A new automatic approach for effectively fusing Landsat 7 as well as IKONOS images. In: Proceedings of the IEEE International Geoscience and Remote Sensing Symposium. Toronto, Ontario, Canada: IEEE, 4: 2429–2431, doi: 10.1109/IGARSS.2002.1026567

Zhang Yun. 2002b. Problems in the fusion of commercial high-resolution satelitte as well as Landsat 7 images and initial solutions. International Archives of Photogrammetry Remote Sensing and Spatial Information Sciences, 34(4): 587–592

Zhu Li, Li Yunmei, Zhao Shaohua, et al. 2015. Remote sensing monitoring of Taihu Lake water quality by using GF-1 satellite WFV data. Remote Sensing for Land & Resources (in Chinese), 27(1): 113–120